Journal of Biomolecular NMR **30:** 327–346, 2004.

Asparagine and glutamine side-chain conformation in solution and crystal: A comparison for hen egg-white lysozyme using residual dipolar couplings

Victoria A. Higman[a,b], Jonathan Boyd[a,c], Lorna J. Smith[a,b] & Christina Redfield[a,b,c,*]
[a]*Oxford Centre for Molecular Sciences;* [b]*Department of Chemistry;* [c]*Department of Biochemistry, University of Oxford, U.K.*

Received 27 July 2004; Accepted 11 August 2004

Key words: asparagine, glutamine, hen egg-white lysozyme, order parameters, residual dipolar couplings, side-chain conformation

Abstract

Experimental ^{15}N–^{1}H and ^{1}H–^{1}H residual dipolar couplings (RDCs) for the asparagine (Asn) and glutamine (Gln) side chains of hen egg-white lysozyme are measured and analysed in conjunction with ^{15}N relaxation data, information about χ^1 torsion angles in solution and molecular dynamics simulations. The RDCs are compared to values predicted from 16 high-resolution crystal structures. Two distinct groups of Asn and Gln side chains are identified. The first contains residues whose side chains show a fixed, relatively rigid, conformation in solution. For these residues there is good agreement between the experimental and predicted RDCs. This agreement improves when the experimental order parameter, S, is included in the calculation of the RDCs from the crystal structures. The comparison of the experimental RDCs with values calculated from the X-ray structures shows that the similarity between the oxygen and nitrogen electron densities is a limitation to the correct assignment of the Asn and Gln side-chain orientation in X-ray structures. In the majority of X-ray structures a 180° rotation about χ^2 or χ^3, leading to the swapping of $N^{\delta/\varepsilon 2}$ and $O^{\delta/\varepsilon 1}$, is necessary for at least one Asn or Gln residue in order to achieve good agreement between experimental and predicted RDCs. The second group contains residues whose side chains do not adopt a single, well-defined, conformation in solution. These residues do not show a correlation between the experimental and predicted RDCs. In many cases the family of crystal structures shows a range of orientations for these side chains, but in others the crystal structures show a well-defined side-chain position. In the latter case, this is found to arise from crystallographic contacts and does not represent the behaviour of the side chain in solution.

Introduction

Asparagine and glutamine residues play important structural roles in proteins because their side-chain amide groups can act as both hydrogen bond acceptors and donors. These hydrogen bonds can stabilise the protein structure particularly through formation of C-capping interactions in helices (Lesk, 2001). In addition, these residues are often found on the surface of proteins or in the active site of enzymes where the hydrogen bonds they form can be important in stabilising protein–protein or protein-substrate interactions. For example, asparagine and glutamine residues have been postulated to play an important role in the interaction of hen egg-white lysozyme (hereafter referred to as hen lysozyme) with the six sugar moieties of the substrate which occupy the active site; Asn 103 is involved in a

*To whom correspondence should be addressed. E-mail: christina.redfield@bioch.ox.ac.uk

hydrogen bond with a hydroxyl group in site A, and Gln 57 and Asn 37 are postulated to interact with hydroxyl groups in sites E and F, respectively (Imoto et al., 1972; Cheetham et al., 1992; Vocadlo et al., 2001).

X-ray crystallography is a powerful method for defining the three-dimensional structures of proteins at atomic resolution. However, for asparagine and glutamine residues structural ambiguities can arise which can make it difficult to identify, with confidence, the structural role of these residues. These uncertainties arise because the electron densities of nitrogen and oxygen atoms in protein electron density maps are very similar. This leads to ambiguity in the identification of the $N^{\delta/\varepsilon 2}$ and $O^{\delta/\varepsilon 1}$ atoms in Asn and Gln side chains and to ambiguity in the χ^2 (C^{α}–C^{β}–C^{γ}–O^{δ}) and χ^3 (C^{β}–C^{γ}–C^{δ}–O^{ε}) torsion angles, respectively. An analysis of hydrogen bonding can give important clues in determining the correct orientation of these side chains in X-ray structures (McRee, 1999). It has been shown that the addition of hydrogen atoms and the consideration of their van der Waal's radii can, in many instances, also be of help in distinguishing between $N^{\delta/\varepsilon 2}$ and $O^{\delta/\varepsilon 1}$ in crystal structures by excluding orientations which would result in bad steric clashes (Word et al., 1999a).

With NMR techniques the side-chain nitrogen and oxygen of asparagine and glutamine can be readily distinguished. The side-chain NH_2 group of Asn and Gln gives rise to observable peaks in ^{15}N–^{1}H HSQC spectra. As a result of hindered rotation about the $C^{\gamma/\delta}$–$N^{\delta/\varepsilon}$ partial double bond, the two protons of the NH_2 group inter-convert slowly on the NMR timescale and give rise to distinct resonances. Information about the position of the NH_2 group in the protein structure can be obtained from observed inter-residue NOE effects arising from these side-chain protons. However, these data can be difficult to interpret as a result of chemical exchange between the two H^N positions and because of the lack of stereo-specific assignment of the two H^N resonances. In this study, we have examined the use of residual dipolar couplings (RDCs) to provide information about the orientation of Asn and Gln side chains in hen lysozyme.

There has been much interest recently in the use of RDC data in NMR protein structure determinations. These data establish the orientation of inter-nuclear vectors with respect to an alignment tensor axis frame in the molecule and so complement the short-range NOE and torsion angle restraints (Tjandra and Bax, 1997; Prestegard, 1998). Significant improvements to the accuracy of NMR structures on inclusion of dipolar coupling restraints have been reported for a number of systems (Bax and Tjandra, 1997; Tjandra et al., 1997; de Alba et al., 1999; Markus et al., 1999; Schwalbe et al., 2001). Backbone ^{15}N–^{1}H RDCs collected in two different bicelle media have been used to refine the solution structure of hen lysozyme (Schwalbe et al., 2001). The spectra from which these backbone dipolar couplings were obtained also contain, in principle, information for the side-chain NH groups of Arg, Asn, Gln, Lys and Trp. Other experiments have been developed recently for the measurement of a number of ^{15}N–^{1}H, ^{13}C–^{1}H and ^{15}N–^{13}C dipolar couplings for Asn and Gln NH_2 groups. These generally require double-labelled protein and stereospecific assignments for the amide protons (Bertini et al., 2000; Cai et al., 2001; Permi, 2001). In this study we focus on the information about Asn and Gln side-chain conformation that can be obtained from the spectra used to measure backbone dipolar couplings for ^{15}N-labelled proteins, using hen lysozyme as an example. These RDCs are analysed in conjunction with ^{15}N relaxation data for the Asn and Gln side chains, with information about χ^1 torsion angles in solution obtained from coupling constant measurements and peak-shape analysis, and with molecular dynamics simulations. In addition, the information about the Asn and Gln side-chain conformation in solution determined from the analysis of RDCs is compared with predicted dipolar couplings calculated from the large number of available crystal structures for hen lysozyme.

Materials and methods

Sample preparation

RDCs were measured for 1.4 mM ^{15}N-labelled hen lysozyme (MacKenzie et al., 1996) in a bicelle solution. This contained 5% w/v 1,2-O-ditridecyl-*sn*-glycero-3-phosphocholine (D13OPC), 1,2-dihexyl-*sn*-glycero-3-phospho-choline(DHOPC), and

cetyl trimethyl ammonium bromide (CTAB), in a ratio [D13OPC]:[DHOPC]:[CTAB] = 30:10:1, in 50 mM KCl at pH 3.5 (93%/7% H_2O/D_2O). The CTAB was added to give the bicelles an overall positive charge. The sample preparation protocol followed that described by Ottiger and Bax (1999). Isotropic $^1J_{NH}$ values were measured for a 1.4 mM sample of ^{15}N-labelled hen lysozyme in 95% H_2O/5% D_2O at pH 3.5.

Measurement of residual dipolar couplings and data analysis

The $^1H–^{15}N$ RDCs were measured from the $^1J_{NH}$ splitting appearing in the ^{15}N dimension of an HSQC experiment which incorporated a S^3E pulse sequence element (Meissner et al., 1997). The experiments were recorded at 750 MHz using 128 (t_1-^{15}N) and 1024 (t_2-^1H) complex points with acquisition times of 28.0 and 99.0 ms, respectively. The data were processed using Felix 2.3 (Accelrys) to give a final digital resolution of 0.277 Hz/pt (F_1) and 5.14 Hz/pt (F_2). A pair of spectra was collected at 35 °C for the D13OPC:DHOPC:CTAB bicelle solution and for an isotropic solution of lysozyme.

Co-ordinates for 56 X-ray and two neutron diffraction structures of hen lysozyme were obtained from the PDB (Berman et al., 2000). Ten of these structures are derived from monoclinic crystals which contain two molecules per unit cell; both structures were used in the analysis and are designated *a* and *b*. The tetragonal 1IEE structure contains alternative conformations for some Asn/Gln side chains; two coordinate sets, designated *a* and *b*, were created to include these alternate side-chain conformations. Average B-factors for each Asn and Gln residue were calculated from the B-factors reported for the $N^{\delta/\varepsilon 2}$ and $O^{\delta/\varepsilon 1}$ atoms in the 14 X-ray structures selected for detailed analysis. Hydrogens were added to the X-ray structures using the HBUILD feature in the program XPLOR (Brünger, 1992). The structures were then energy minimised with all non-hydrogen atoms constrained to their initial positions, as described previously (Boyd and Redfield, 1998), so that the backbone H^N was located in the peptide plane and the Asn and Gln side-chain $CONH_2$ groups were planar. The hydrogen positions reported for the two neutron structures were used. Energy minimisation was carried out to ensure planar side chain amide groups. This was particularly important for Asn 39 of the 1LZN structure (Bon et al., 1999). In the analysis described an ensemble of 50 NMR structures for hen lysozyme that were refined with two sets of backbone $^1H–^{15}N$ residual dipolar couplings (PDB code 1E8L (Schwalbe et al., 2001)) and structures taken from a 1000 ps molecular dynamics simulation of hen lysozyme in water (simulation W2 in Smith et al. (1995)) were also used.

The measured HSQC spectra contain residual dipolar coupling information for both backbone $^1H^N–^{15}N$ and for side-chain $^1H^N–^{15}N$ groups. The RDC for backbone $^1H^N–^{15}N$ is taken as the difference between the splitting observed in the bicelle and isotropic solutions ($D_{NH} = {}^1J_{NH}(bic) - {}^1J_{NH}(iso)$). In the case of the Asn and Gln side-chain NH_2 groups, the splitting observed in the ^{15}N dimension of the HSQC spectra, which incorporate a S^3E pulse sequence element, is the sum of the contributions from the two amide protons ($^1J_{obs} = {}^1J_{NH1} + {}^1J_{NH2}$), and the RDC that is measured represents the sum of the contributions from the two H^N ($D_{obs} = D_{NH1} + D_{NH2}$). Both the low and high field components of the doublet are observed in each of the spectra collected since the pulse sequence delays have been optimised for the backbone amide splitting of ~ -95 Hz. The pair of peaks observed for each NH_2 group and the observation of both the low and high field doublet components in each of the spectra collected allowed up to four values for each RDC sum to be measured. These four measurements were used to estimate the experimental error. The $^1H–^1H$ RDC for the Asn and Gln side chains were measured from the observed splittings in the F_2 (^1H) dimension of an HSQC spectrum which had been zero-filled to give a digital resolution of 1.28 Hz/pt in F_2. A lineshape fitting program was used to account for the effects of finite linewidths and window functions. Splittings of less than about 10 Hz could not generally be resolved. The reported values have not been corrected for the ^2J value of $\sim$2 Hz between the two amide protons.

The principle components (A_{xx}, A_{yy} and A_{zz}) and orientation (ϕ, θ and Ψ) of the molecular alignment tensor for each X-ray or neutron structure were fitted to minimize the χ^2 between the

experimental and calculated RDCs for a group of 93 backbone amides. Residues with S^2 values, determined from ^{15}N relaxation analysis, of less than 0.7 were excluded from the analysis. The fitted values of the principle components and orientation of the alignment tensor were then used to calculate the pair of RDCs expected for the Asn and Gln side-chain $^1H^N$–^{15}N and the sum of the two values calculated as well as the $^1H^{\delta/\varepsilon}$–$^1H^{\delta/\varepsilon}$ RDCs. The N–H bond length in the amide group was assumed to be 1.02 Å. The same process was used to predict RDCs for a family of NMR structures (Schwalbe et al., 2001) and for structures from a molecular dynamics simulation (Smith et al., 1995). The $CONH_2$ groups of some Asn and Gln side chains were rotated by 180° about the χ^2 and χ^3 torsion angles, respectively, and the RDCs for these residues were then recalculated. Contributions to the ^1H–^1H RDCs from other protons in the vicinity of the Asn or Gln side chains were calculated for the crystal structures. These values were generally substantially smaller than the geminal ^1H–^1H RDC and were not found to contribute significantly to the predicted RDCs. These contributions are not included in Tables 1–3.

Results and discussion

Measurement of residual dipolar couplings

RDCs were measured for ^{15}N-labelled hen lysozyme in an ether bicelle solution as described in the Materials and methods section. The Asn and Gln side-chain region of the pair of HSQC spectra, which incorporate a S^3E pulse sequence element (Meissner et al., 1997), is shown in Figure 1. The spectra contain RDC information for both backbone and side-chain $^1H^N$–^{15}N groups. The RDC for a backbone $^1H^N$–^{15}N is measured as the difference between the splitting observed in bicelle and isotropic solutions. For the Asn and Gln side-chain NH_2 groups, the splitting observed in the ^{15}N dimension is the sum of the contributions from the two amide protons and the RDC that is measured represents the sum of the contributions from the two H^N. It is also clear from Figure 1 that for some Asn and Gln side chains (in particular, Asn 37, Asn 46, Asn 65, Asn 113 and Gln 121) a large splitting is observed in the ^1H dimension (F_2). This represents a large ^1H–^1H RDC between the two H^δ or H^ε of Asn or Gln, respectively. As the distance between this pair of protons is fixed, this homonuclear RDC can also provide structural information. However, the sign of this coupling cannot be determined from the spectra collected in this study. For each Asn and Gln side chain of lysozyme the sum of the pair of $^1H^N$–^{15}N dipolar couplings and the absolute value of the $^1H^N$–$^1H^N$ dipolar coupling were measured and are summarised in Tables 1–3.

Prediction of residual dipolar couplings from X-ray structures

Hen lysozyme is one of the most studied and best characterised globular proteins. It was the first enzyme to have its structure determined by X-ray crystallography (Blake et al., 1965). Hen lysozyme has been used extensively as a model system in protein crystallography studies because of the availability of large quantities of inexpensive very pure protein, its relative ease of crystallisation and the wealth of other biophysical data available for this protein. These studies have been aimed at assessing factors such as crystallisation and data collection methods, the effects of zero gravity on crystallisation, the effects of different salts, pH, pressure, temperature and many other factors. As a result, there are 56 X-ray diffraction co-ordinate sets for hen lysozyme, 48 being of 2 Å or better resolution, deposited in the Brookhaven Protein Data Bank (PDB) (Berman et al., 2000). Due to multiple molecules per unit cell in some crystal forms this gives a total of 66 structures. There are few other proteins for which such a large number of high resolution crystal structures is available.

Hen lysozyme crystallises in four forms, monoclinic, orthorhombic, tetragonal and triclinic, and several examples of each of these can be found in the PDB. In order to assess how well each of these X-ray structures describes hen lysozyme in solution, the dipolar couplings measured for 93 of the 129 backbone amides were compared to values calculated from the 66 X-ray structures. The principle components (A_{xx}, A_{yy} and A_{zz}) and orientation (ϕ, θ and Ψ) of the molecular alignment tensor for each X-ray structure were fitted to minimize the χ^2 between experimental and calculated RDCs for the 93

Table 1. Experimental and predicted residual dipolar couplings for Asn and Gln residues with $S^2 > 0.7$

		X-ray													Neutron	
PDB code[a]		1RFP	193L	1HEL	1LSC	1LZA	1DPX	1AZF	1IEEb	1LKS	4LZT	1AKI	1BGI	5LYMa	5LYMb	1LZN	1IO5
Crystal type[b]		tet	tet	tet	tet	tet	tet	Tet	tet	tri/cl	tri/cl	o/rhom	o/rhom	m/cl	m/cl	tri/cl	tet
Q-value[c]		0.15	0.16	0.16	0.16	0.17	0.18	0.20	0.20	0.18	0.18	0.19	0.20	0.20	0.19	0.20	0.56
Resolution (Å)		1.8	1.3	1.7	1.7	1.6	1.6	1.8	0.9	1.1	1.0	1.5	1.7	1.8	1.8	1.7	2.0
Temp. of collection (K)		295	279	–	250	282	100	297	110	–	295	298	283	293	293	295	–
Experimental RDCs[d]		**RDCs predicted from Crystal Structures[e]**															
$\Sigma^{15}N$–^1H RDCs (Hz)																	
Asn 27	−9.2 ± 0.2	**−8.8**	**−9.0**	**−9.5**	**−8.5**	**−8.4**	**−9.4**	−4.1	**−8.9**	**−10.6**	**−10.9**	**−9.3**	**−11.3**	**−12.2**	**−11.1**	**−11.4**	**−3.7**
(rotated)		4.0	4.0	2.8	7.6	4.7	2.2	**−7.7**	2.4	−1.1	−1.8	0.3	−1.6	−4.2	−1.4	−0.8	2.3
Asn 39	−8.0 ± 0.5	**−8.3**	**−9.4**	**−6.2**	**−6.6**	**−5.6**	**−12.8**	**−9.1**	**−10.9**	**−7.4**	**−9.3**	**−6.1**	**−11.2**	**−4.0**	5.2	**−9.7**	**−10.9**
(rotated)		−2.9	−4.1	−1.9	1.0	−3.8	−14.5	−3.9	−12.9	−5.2	−6.9	−17.1	−19.8	5.9	**−6.3**	−7.2	−13.6
Gln 57	13.6 ± 0.4	**9.6**	**11.3**	**11.1**	**9.9**	**8.7**	**10.8**	**5.8**	**10.3**	**8.0**	**9.3**	**10.3**	**7.9**	**10.1**	−2.6	**10.6**	**10.9**
(rotated)		−4.4	−3.4	−1.4	−6.3	−1.9	−4.3	−2.8	−4.9	1.0	−0.4	−4.4	−4.7	−3.5	**10.4**	−2.0	3.2
Asn 59	19.4 ± 0.0	**24.7**	**24.3**	**23.6**	*16.6*	**23.5**	**23.8**	**25.3**	**25.1**	**24.1**	**24.0**	**23.3**	**24.1**	5.4	**25.2**	**24.1**	*−5.6*
(rotated)		5.0	6.5	4.4	*0.5*	3.6	3.2	4.0	−1.5	5.6	6.8	5.8	4.4	**24.2**	6.6	7.2	*−9.0*
Asn 74	14.9 ± 0.3	**21.9**	**23.1**	**20.4**	**20.8**	−7.5	**23.6**	−10.0	**20.7**	**18.7**	**19.3**	**22.1**	**20.8**	−9.2	−11.3	**18.9**	**15.1**
(rotated)		−1.9	−2.0	−3.2	−4.2	**26.3**	−2.4	**20.3**	−0.5	−3.1	−2.5	−2.6	−2.5	**28.1**	**27.3**	−2.4	−5.1
^1H–^1H RDCs (Hz)																	
Asn 27	±22.9	**−16.2**	**−17.0**	**−16.2**	**−16.6**	**−16.2**	**−17.1**	−1.2	**−16.4**	**−15.2**	**−14.9**	**−13.7**	**−16.7**	**−16.0**	**−16.3**	**−15.6**	**−2.9**
(rotated)		8.1	7.5	7.0	13.8	8.7	4.9	**−11.4**	4.9	2.9	2.3	4.6	1.6	−0.9	2.0	3.4	7.9
Asn 39	< ±10	**−7.9**	**−9.2**	**−4.3**	**−7.4**	**−2.7**	**−9.4**	**−8.9**	**−7.1**	**−5.0**	**−7.8**	**0.4**	**−4.5**	**−5.9**	12.0	**−8.4**	**−7.2**
(rotated)		2.2	0.9	3.8	7.0	0.8	−12.5	0.9	−11.0	−1.0	−3.1	−20.4	−20.9	12.8	**−9.8**	−3.5	−12.5
Gln 57	±21.2	**17.9**	**20.1**	**19.8**	**18.4**	**16.5**	**19.5**	**12.8**	**18.7**	**15.6**	**17.2**	**18.9**	**15.8**	**18.2**	−5.7	**19.0**	**19.6**
(rotated)		−8.5	−7.5	−3.7	−12.0	−3.5	−8.9	−3.3	−10.0	−1.2	−1.1	−8.9	−7.8	−7.2	**18.8**	−3.2	−3.0
Asn 59	±37.6	**39.9**	**39.2**	**38.5**	*25.8*	**38.6**	**39.2**	**40.7**	**37.1**	**38.9**	**38.8**	**38.1**	**39.3**	3.9	**40.2**	**38.9**	*−11.8*
(rotated)		2.7	5.4	2.2	*−4.8*	0.9	0.2	0.3	−13.1	4.0	6.4	5.0	2.1	**39.4**	5.0	6.8	*−19.9*
Asn 74	±21.3	**29.9**	**32.0**	**28.2**	**29.4**	−20.2	**33.0**	−21.3	**28.4**	**25.3**	**26.1**	**30.3**	**27.8**	−18.1	−20.7	**25.7**	**20.5**
(rotated)		−15.0	−15.3	−16.5	−17.9	**36.6**	−16.2	**29.1**	−11.7	−15.9	−15.2	−16.3	−16.2	**40.8**	**39.2**	−14.8	−15.5

[a]The four letter PDB codes for the X-ray and neutron structures are given. The letters *a* or *b* following the four letter code indicate that models *a* or *b* from the PDB file have been used. The literature references for the crystal structures are 1RFP (Motoshima et al., 1997), 193L (Vaney et al., 1996),1HEL (Wilson et al., 1992), 1LSC (Kurinov and Harrison, 1995), 1LZA (Maenaka et al., 1995), 1DPX (Weiss et al., 2000), 1AZF (Lim et al., 1998), 1IEEb (Sauter et al., 2001), 1LKS (Steinrauf, 1998), 4LZT (Walsh et al., 1998), 1AKI (Artymiuk et al., 1982), 1BGI (Oki et al., 1999), 5LYMa and b (Rao and Sundaralingam, 1996), 1LZN (Bon et al., 1999) and 1IO5 (Niimura et al., 1997).

[b]Crystal forms are tetragonal (tet), triclinic (tri/cl), orthorhombic (o/rhom) and monoclinic (m/cl).

[c]Q-values were calculated as described by Cornilescu et al. (1998) using 93 backbone RDCs.

[d]The sum of the two ^{15}N–^1H RDCs and the ^1H–^1H RDCs are shown. The sign of the ^1H–^1H RDC cannot be determined.

[e]RDCs have been predicted for the side chain orientation observed in the crystal structures (1st row) and for the side chain orientation that results from a 180° rotation of the $CONH_2$ group about χ^2 or χ^3 (2nd row). Values in bold are in agreement with the solution RDC data, values in italics indicate that the side chain has a fundamentally different orientation to the other structures (not simply rotated by 180°).

Table 2. Experimental and predicted residual dipolar couplings for Asn and Gln residues with $S^2 < 0.5$

Experimental RDCs[a]		**RDCs predicted from crystal structures**[b]														
		X-ray													**Neutron**	
		1RFP[c]	193L	1HEL	1LSC	1LZA	1DPX	1AZF	1IEEb	1LKS	4LZT	1AKI	1BGI	5LYMa	5LYMb	1LZN	1IO5
Σ^{15}N–^{1}H RDCs (Hz)																	
Gln 41	−5.6 ± 0.1	4.9	5.4	6.9	−5.3	6.5	6.8	5.6	5.7	−11.7	−23.6	8.5	−2.6	−7.4	2.1	−24.5	6.1
Asn 77	4.3 ± 0.0	24.7	24.0	−3.4	5.4	25.8	−2.7	17.1	8.6	17.7	19.7	27.2	20.0	15.9	19.7	17.6	1.8
Asn 103	0.8 ± 0.1	−10.5	4.4	25.7	4.3	−4.1	−1.8	10.4	−3.6	13.8	23.4	1.5	−15.4	9.5	−14.3	24.1	0.5
Asn 113	−7.1 ± 0.2	1.3	1.3	−0.9	29.1	0.2	1.2	1.4	0.6	5.4	1.7	7.5	4.8	28.4	2.9	1.7	−2.8
Gln 121	11.9 ± 0.1	10.5	−5.2	20.1	17.0	−21.6	−0.8	4.2	−6.3	−0.5	16.6	−17.8	−0.7	−7.2	15.9	16.3	17.8
^{1}H–^{1}H RDCs (Hz)																	
Gln 41	< ±10	1.7	2.8	5.6	−19.2	4.7	5.5	1.4	3.8	−19.8	−26.1	17.6	−2.7	−7.8	−8.9	−27.2	6.8
Asn 77	< ±5	37.8	38.9	−16.5	3.2	40.3	−11.4	25.4	8.4	27.2	29.7	37.5	28.8	25.3	25.5	27.0	−5.7
Asn 103	< ±5	−6.0	−1.9	40.3	9.8	−18.2	−13.5	17.6	−15.3	15.7	30.8	−1.2	−19.4	8.3	−11.5	31.8	−7.8
Asn 113	±19.2	−8.6	−8.5	−11.9	44.7	−10.0	−8.5	−7.8	−9.2	0.2	−7.0	4.8	−1.2	43.2	−4.2	−6.8	−14.6
Gln 121	±19.9	6.1	−2.3	25.6	30.6	−23.1	2.1	8.5	−7.6	−7.9	21.7	−22.1	4.8	−5.4	21.8	21.2	26.6

[a]The sum of the two ^{15}N–^{1}H RDCs and the ^{1}H–^{1}H RDCs are shown. The sign of the ^{1}H–^{1}H RDC cannot be determined.
[b]RDCs have been predicted for the side chain orientation observed in the crystal structures.
[c]The four letter PDB codes for the X-ray and neutron structures are given. The letters *a* or *b* following the four letter code indicate that models *a* or *b* from the PDB file have been used.

Table 3. Experimental and predicted residual dipolar couplings for Asn and Gln residues with intermediate S^2 values

Experimental RDCs[a]		**RDCs predicted from crystal structures**[b]														
		X-ray													**Neutron**	
		1RFP[c]	193L	1HEL	1LSC	1LZA	1DPX	1AZF	1IEEb	1LKS	4LZT	1AKI	1BGI	5LYMa	5LYMb	1LZN	1IO5
$\Sigma^{15}N$–^1H RDCs (Hz)																	
Asn 19	−5.3 ± 0.1	21.6	5.7	3.1	1.5	4.4	2.3	−2.7	4.9	−17.3	−16.3	−22.0	24.6	2.6	3.6	−16.8	−3.8
Asn 37	14.3 ± 0.1	**22.6**	**20.9**	**18.7**	−7.1	**22.7**	**22.1**	**17.9**	**22.5**	**22.7**	**21.5**	**24.8**	**18.9**	**24.0**	−4.8	*11.7*	**23.9**
(rotated)		−5.0	−4.8	−1.8	**20.3**	−1.8	−2.6	−6.3	0.6	−1.4	2.2	−1.7	−3.4	−3.8	**17.4**	*−10.2*	−4.2
Asn 44	2.8 ± 0.3	−4.9	22.9	−2.7	22.7	−6.1	−6.0	−5.8	−4.9	−17.4	−17.0	−18.0	−21.7	18.5	−18.4	−12.8	−11.1
Asn 46	23.1 ± 0.2	**29.1**	8.9	8.1	5.4	10.8	4.4	6.5	**29.2**	**26.9**	**26.0**	16.1	**29.4**	**27.8**	**26.3**	**25.8**	**22.2**
(rotated)		12.9	**29.7**	**29.1**	**29.1**	**30.2**	**28.7**	**29.1**	9.3	15.0	12.4	**29.0**	18.2	16.2	16.6	12.2	7.6
Asn 65	15.5 ± 0.2	**25.0**	**23.5**	**23.2**	**22.2**	**22.7**	**22.6**	17.6	**21.2**	**23.1**	**22.8**	**22.1**	**21.2**	11.5	**19.6**	**24.1**	**13.0**
(rotated)		7.0	16.8	12.1	13.4	12.4	11.7	**22.4**	7.9	22.9	20.9	13.4	16.7	**17.2**	15.4	19.2	13.8
Asn 93	19.1 ± 0.2	0.1	**26.3**	0.9	**28.2**	**26.1**	−2.5	−1.6	**21.1**	**21.8**	**21.4**	0.6	**24.6**	−0.1	−1.4	**22.7**	**19.4**
(rotated)		**24.6**	0.9	**24.9**	2.3	3.4	**20.3**	**19.9**	−1.6	−2.7	−1.5	**22.8**	0.1	**26.9**	**23.3**	−1.7	−1.8
Asn 106	6.7 ± 0.3	11.2	10.1	10.2	4.6	12.2	8.8	11.6	7.6	*1.6*	1.2	5.6	−3.5	6.0	11.1	−2.9	−10.2
(rotated)		3.4	3.8	6.4	7.4	5.1	3.8	4.3	3.5	*17.7*	4.7	5.6	8.3	0.0	7.1	7.5	21.0
^1H–^1H RDCs (Hz)																	
Asn 19	±7.2	32.4	4.8	−1.5	−4.4	−3.0	−4.6	−11.9	−0.7	−18.0	−17.4	−19.8	36.9	−4.9	−4.9	−18.1	−11.4
Asn 37	±28.6	**37.2**	**35.5**	**32.6**	−16.3	**38.1**	**37.2**	**31.6**	**37.5**	**37.3**	**36.4**	**39.9**	**32.8**	**39.5**	−17.2	*31.0*	**37.8**
(rotated)		−14.9	−13.0	−6.1	**34.0**	−8.3	−9.5	−14.2	−3.9	−8.1	−0.1	−10.2	−9.3	−13.0	**39.3**	*−18.9*	−15.1
Asn 44	< ±5	−16.0	37.2	−12.0	36.4	−17.4	−17.4	−17.2	−15.3	−15.7	−15.2	−17.2	−19.8	28.4	−15.5	−10.1	−19.5
Asn 46	±38.0	**42.8**	5.2	3.7	−1.2	7.6	−2.8	0.5	**43.3**	**39.3**	**37.4**	17.6	**41.6**	**40.9**	**38.5**	**37.0**	**33.9**
(rotated)		12.2	**44.5**	**43.5**	**43.7**	**44.3**	**43.2**	**43.2**	5.8	16.7	11.9	**42.0**	20.4	19.1	20.2	11.7	3.5
Asn 65	±27.5	**37.9**	**33.4**	**34.4**	**32.4**	**33.7**	**34.2**	22.6	**32.9**	**32.1**	**31.8**	**33.2**	**30.3**	12.5	**29.0**	**33.6**	**13.3**
(rotated)		4.1	20.7	13.4	15.8	14.2	13.5	**31.7**	7.8	31.7	28.3	16.7	21.7	**23.8**	21.0	25.9	22.3
Asn 93	±33.6	−11.2	**37.1**	−10.8	**40.1**	**37.1**	−13.8	−11.1	**30.7**	**31.5**	**30.7**	−8.7	**34.6**	−13.0	−12.6	**32.6**	**25.3**
(rotated)		**35.4**	−11.0	**35.2**	−9.1	−6.0	**29.4**	**30.0**	−12.3	−14.7	−12.5	**34.0**	−11.8	**38.2**	**34.5**	−12.5	−15.5
Asn 106	< ±10	22.0	20.2	20.2	5.9	23.5	18.1	22.2	16.2	*−2.3*	5.2	12.3	−2.5	14.3	20.3	−0.1	−16.9
(rotated)		7.1	8.3	13.1	16.2	10.1	8.7	8.3	8.5	*28.2*	11.7	12.4	19.6	2.9	12.7	15.3	35.2

[a]The sum of the two ^{15}N–^1H RDCs and the ^1H–^1H RDCs are shown. The sign of the ^1H–^1H RDC cannot be determined.

[b]For Asn 37, 46, 65, 93 and 106, the RDCs have been predicted for the side chain orientation observed in the crystal structures (1st row) and for the side chain orientation that results from a 180° rotation of the $CONH_2$ group about χ^2 or χ^3 (2nd row). Values in bold are in agreement with the solution RDC data, values in italics indicate that the side chain has a fundamentally different orientation to the other structures (not simply rotated by 180°). For Asn 19 and 44, the RDCs have been predicted only for the side chain orientation observed in the crystal structures.

[c]The four letter PDB codes for the X–ray and neutron structures are given. The letters *a* or *b* following the four letter code indicate that models *a* or *b* from the PDB file have been used.

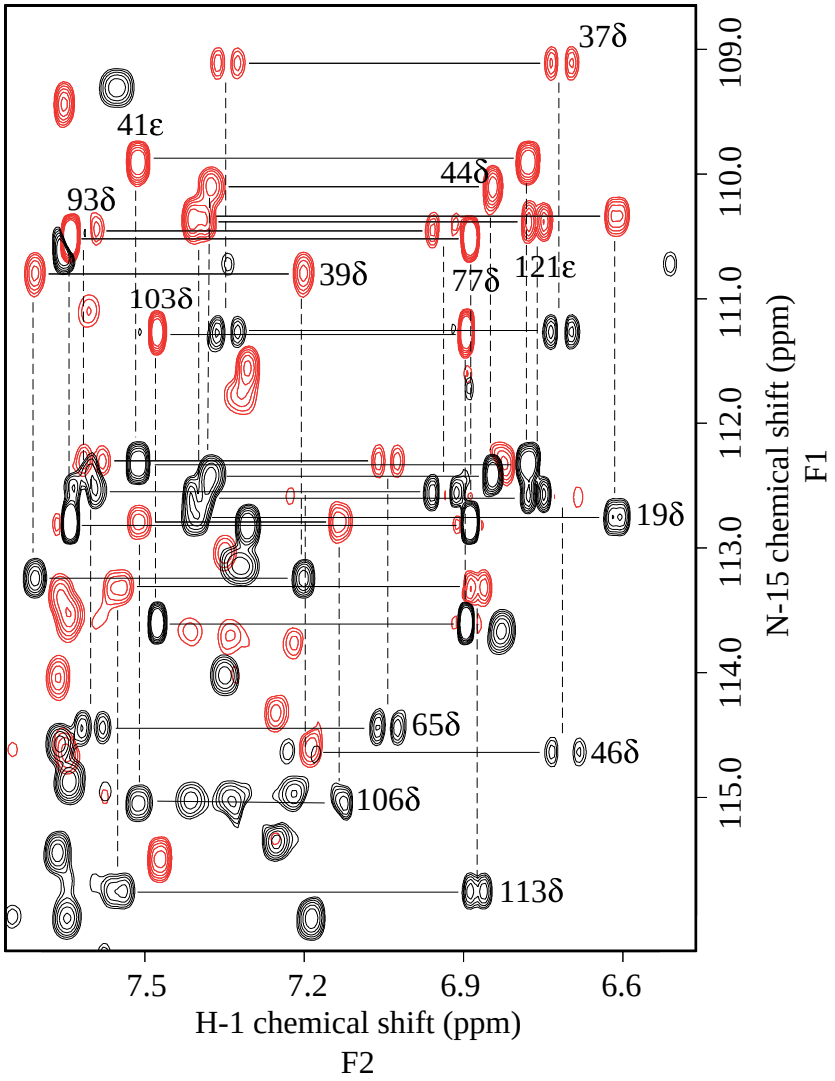

Figure 1. Superposition of two ^{15}N–^{1}H HSQC spectra which incorporated a S^3E pulse sequence element; only positive peaks are shown. These spectra of hen lysozyme were recorded at 750 MHz in a 5% ether bicelle solution. The side-chain peaks of 13 of the 17 Asn/Gln residues are labelled. The peaks arising from Asn 27, 59, 74 and Gln 57 have $^{1}H^{N}$ and/or ^{15}N chemical shifts outside the spectral region illustrated.

backbone amides. *Q*-values (Cornilescu et al., 1998) were evaluated for each structure; these ranged from 0.15 to 0.67. Generally, the lowest *Q*-values were found for structures of tetragonal crystals. Fourteen X-ray and two neutron structures were then chosen for closer analysis. Structures were selected on the basis of having a low *Q*-value and being of high resolution (1.8 Å or better). In addition, at least one structure was selected for each of the four crystal forms. The fitted values of the principle components and orientation of the alignment tensor were then used to calculate, for each these 16 structures, the sum of the pair of RDCs expected for the Asn and Gln side-chain ^{1}H–^{15}N groups, and the ^{1}H–^{1}H dipolar coupling expected for H^{δ} and H^{ε} of the Asn and Gln residues, respectively; these predicted RDCs are listed in Tables 1–3.

^{15}N relaxation methods have been used previously to study the dynamics of the asparagine and glutamine side chains of hen lysozyme (Buck et al., 1995). Order parameters, S^2, ranging from 0.19 to

0.82 were reported indicating a large variation in the magnitude of fast time-scale dynamics for the 17 asparagine and glutamine side chains in hen lysozyme. The experimental and predicted RDCs for these residues will be discussed in the light of the previously observed dynamic behaviour.

Comparison of experimental and predicted RDCs for Asn/Gln side chains with $S^2 > \sim 0.7$

The first group of residues to be analysed are those whose side chains are known from the relaxation study to have a similar mobility to the backbone amides, that is residues with a heteronuclear NOE ratio of $> \sim 0.75$ and $S^2 > \sim 0.7$. In hen lysozyme these are Asn 27, Asn 39, Gln 57, Asn 59 and Asn 74 (Buck et al., 1995). The RDCs predicted for these side chains in the 14 X-ray structures are shown in Table 1. Most X-ray structures were found to give predicted sums of $^1H^N$–^{15}N dipolar couplings that are in reasonable agreement with the experimental data. The predicted values are often of larger magnitude than the experimental values; this observation will be discussed later. There is also generally good agreement for the magnitude of the ^1H–^1H RDCs. For some residues, however, clear discrepancies are observed. For Gln 57, the 5LYMb structure predicts a value of −2.6 Hz which is significantly different from the experimental value of +13.6 Hz. This structure also predicts a much smaller ^1H–^1H dipolar coupling (−5.7 Hz) for Gln 57 than is observed experimentally (±21.2 Hz). Similar discrepancies are observed for Asn 27 in the 1AZF structure, for Asn 39 in the 5LYMb structure, for Asn 59 in the 5LYMa structure, and for Asn 74 in the 1LZA, 1AZF, 5LYMa and 5LYMb structures.

This observation prompted a closer inspection of the family of crystal structures for these residues. Most structures overlaid very well, as shown in Figure 2a, but in some cases χ^2 for Asn and χ^3 for Gln were found to be rotated by 180°, in effect swapping the positions of the $N^{\delta/\varepsilon 2}$ and $O^{\delta/\varepsilon 1}$ atoms. A direct correlation is found between those structures in which the calculated RDCs do not agree with the experimental data and those in which χ^2 or χ^3 is rotated by 180° compared to the majority of structures. If the $CONH_2$ groups of these Asn or Gln residues are rotated by 180° about χ^2 or χ^3, respectively, and the RDCs are recalculated, then good agreement is obtained as shown in Table 1. Conversely, if the side chains of residues giving good agreement between experimental and calculated values are rotated by 180° then poor agreement is found. The Asn 59 side chain in the 1LSC structure is a slight anomaly as it does not overlay very well with the other structures, and so here the discrepancy is not simply due to a 180° rotation about χ^2.

The similarity in the electron densities of nitrogen and oxygen can lead to ambiguity in the identification of the $N^{\delta/\varepsilon 2}$ and $O^{\delta/\varepsilon 1}$ atoms of Asn and Gln side chains in X-ray structures. Analysis of hydrogen bonding is often used to determine the correct orientation of these side chains. In hen lysozyme the side chains of Asn 27, Asn 39, Gln 57 and Asn 59 are found to be involved in hydrogen bond interactions which allow the positions of the $N^{\delta/\varepsilon 2}$ and $O^{\delta/\varepsilon 1}$ atoms to be identified unambiguously (Imoto et al., 1972). The X-ray structures for which discrepancies between experimental and predicted dipolar couplings are observed are found to lack these stabilising hydrogen bonds; rotation by 180° about χ^2 or χ^3 results in their formation. For Asn 74 potential hydrogen bonds of approximately equal energy can be identified for both orientations of the $CONH_2$ group. The orientation that is found to give good agreement with the dipolar coupling data has a hydrogen bond between Asn 74 $O^{\delta 1}$ and Ile 78 N. The orientation that is found to give poor agreement has a hydrogen bond between Asn 74 $N^{\delta 2}$ and Ile 78 CO. Ile 78 CO is involved in a hydrogen bond, in all structures, with Asn 65 N in a region of parallel β-sheet; Ile 78 N is not involved in a main-chain hydrogen bond. It may be for this reason that the orientation of the Asn 74 side chain which results in the formation of the hydrogen bond between Asn 74 $O^{\delta 1}$ and Ile 78 N is favoured.

When adding the hydrogen atoms to crystal structures using the program XPLOR (Brünger, 1992) it is necessary to carry out an energy minimisation to ensure that the planar geometry of the $CONH_2$ group is achieved. During this process it was found that those structures whose Asn 27, 39, 59, 74 and Gln 57 side chains appeared to be rotated by 180° produced bad steric clashes between their H^{δ} and H^{ε} atoms and other heavy atoms. The program Reduce (Word et al., 1999a)

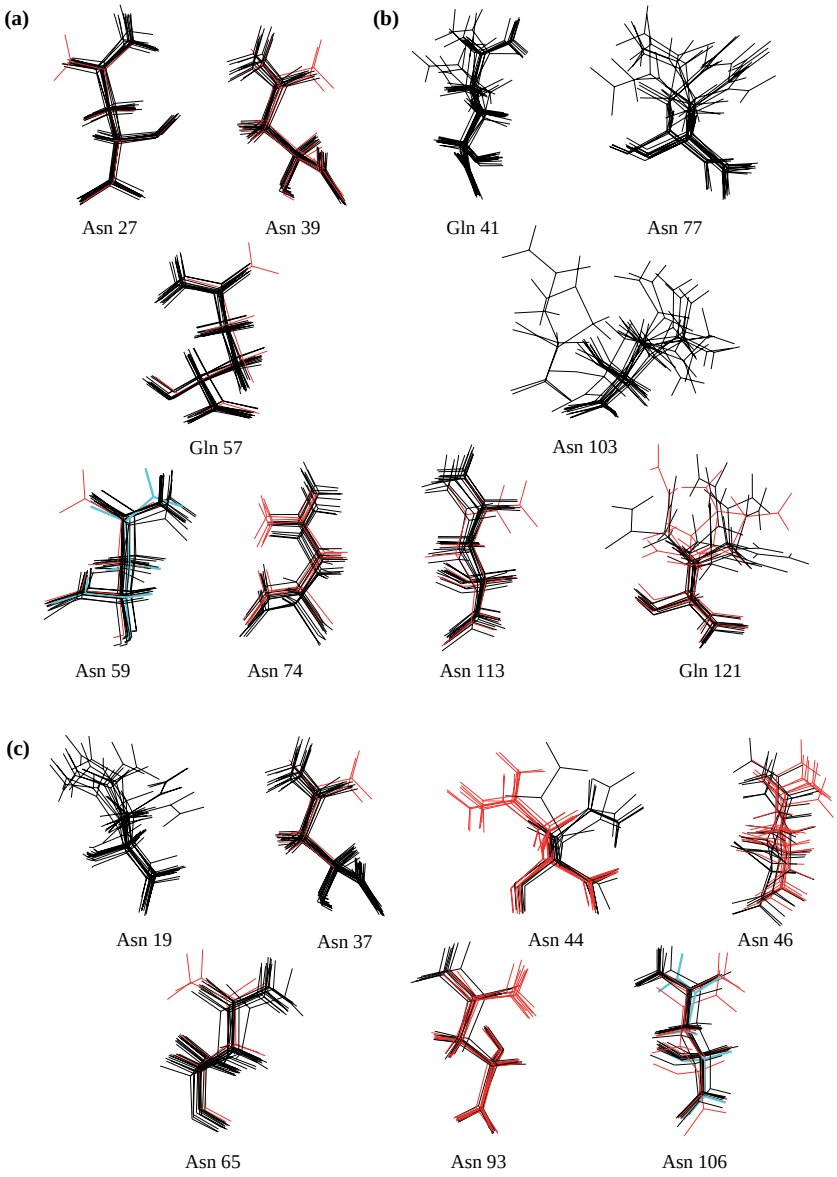

Figure 2. Super position of the Asn and Gln residues in X-ray structures of hen lysozyme. A global superposition of residues 1–129 in 14 X-ray crystal structures was performed using MOLMOL (Koradi et al., 1996). (a) Residues with $S^2 > 0.7$ and a heteronuclear NOE ratio > 0.75. Side chains for which the predicted ^{15}N–^{1}H and ^{1}H–^{1}H RDCs match the experimental RDCs are shown in black; side chains for which a 180° rotation about χ^2 or χ^3 is required are shown in red. The Asn 59 side chain of the 1LSC structure is shown in blue because it has a slightly anomalous orientation. (b) Residues with $S^2 < 0.5$ and a heteronuclear NOE ratio of close to zero or negative. The 1LSC and 5LYMa structures which are rotated by 180° relative to the other crystal structures for Asn 113 are shown in red. Side chains for which the predicted ^{15}N–^{1}H and ^{1}H–^{1}H RDCs match the experimental RDCs for Gln 121 are shown in red. (c) Residues with $0.4 < S^2 < 0.7$ and a heteronuclear NOE ratio between 0.3 and 0.7. Side chains for which the predicted ^{15}N–^{1}H and ^{1}H–^{1}H RDCs match the experimental RDCs for Asn 37, Asn 46, Asn 65 and Asn 93 are shown in black; side chains for which a 180° rotation about χ^2 or χ^3 is required are shown in red. For Asn 44 the tetragonal structures are shown in red. For Asn 106 the 1LSC, 4LZT and 1BGI structures which are rotated by 180° relative to the other crystal structures are shown in red; the Asn 106 1LKS structure is shown in blue because it has a slightly anomalous orientation.

adds hydrogen atoms to crystal structures (with planar geometry) and then specifically looks for Asn H^{δ} and Gln H^{ε} steric clashes and suggests 180° rotations about χ^2 or χ^3 for Asn or Gln side chains if necessary. Reduce not only selects the same side-chain orientations as the RDC data in

all instances for the Asn 27, 39, 59, 74 and Gln 57 side chains, but in conjunction with the programs Probe (Word et al., 1999b) and Mage (Richardson and Richardson, 1992, 1994) also shows that in the cases where the orientation is incorrect, severe steric clashes or overlap occur upon adding hydrogen atoms.

A good correlation between experimental order parameters, S^2, and crystallographic B-factors has been reported for the Asn and Gln side chains of hen lysozyme (Buck et al., 1995). The five Asn and Gln residues discussed above have relatively low B-factors for $N^{\delta/\varepsilon 2}$ and $O^{\delta/\varepsilon 1}$; average values ranging from 12.4 ± 3.0 Å^2 to 18.9 ± 6.9 Å^2 are observed in the family of 14 X-ray structures. The side-chain B-factors observed for Asn and Gln residues which require a 180° rotation about χ^2 or χ^3 are close to the average B-factors observed for these residues in the X-ray structures. For example, the value of 13.8 Å^2 observed for Gln 57 in the 5LYMb structure is close to the average value of 12.4 ± 3.0 Å^2. Therefore, increased side-chain mobility is not responsible for the interchange of the $N^{\delta/\varepsilon 2}$ and $O^{\delta/\varepsilon 1}$ atoms observed for Asn and Gln residues in several X-ray structures.

Neutron diffraction provides a method for the unambiguous identification of the positions of the $N^{\delta/\varepsilon 2}$ and $O^{\delta/\varepsilon 1}$ atoms of Asn and Gln. Hydrogen and deuterium atoms have very different neutron scattering cross sections and, therefore, the positions of these atoms can be identified in neutron diffraction structures (Mason et al., 1984). This method is not widely used for protein structure determination as it requires larger crystals and longer data collection times. However, four neutron diffraction studies of hen lysozyme have been described in the literature (Mason et al., 1984; Niimura et al., 1997; Bon et al., 1999; Ho et al., 2001) and two of the resulting structures, one triclinic and one tetragonal, are deposited in the PDB (Niimura et al., 1997; Bon et al., 1999). Asn and Gln side-chain dipolar couplings have been calculated for these two structures and are shown in Table 1. The triclinic 1LZN structure is found to give good agreement with the data for all five residues. In describing the 1LZN structure, Bon et al. (1999) state that they have looked specifically at the Asn and Gln side chains to ensure the correct location of the amide nitrogen and carbonyl oxygen. The tetragonal 1IO5 neutron structure, however, does not give such good agreement for the Asn and Gln residues (Niimura et al., 1997). Poor agreement between experimental and calculated values is observed for Asn 27 and Asn 59. Rotation by 180° about the χ^2 angle does not improve the agreement. This structure also gives rather poor agreement with the backbone dipolar couplings (Q-value = 0.56), and it can be concluded that 1IO5 does not represent a good model of the structure of lysozyme in solution.

Analysis of the RDC data for the five Asn and Gln residues that show heteronuclear NOE ratios of $> \sim 0.75$ and S^2 values of $> \sim 0.7$ indicates that these data are consistent with a fixed orientation for the $CONH_2$ moiety. This agrees with the observation from E.COSY spectra and COSY peak-shape analysis that these five residues have fixed χ^1 torsion angles in solution (Smith et al., 1991; Bartik and Redfield, 1993). In addition, molecular dynamics simulations show these side chains to have essentially fixed χ^1 and χ^2 torsion angles (Smith et al., 1995).

The orientations of these five Asn and Gln side chains are not well defined in the recently published solution structure of hen lysozyme (PDB code 1E8L) (Schwalbe et al., 2001). This is the result of a lack of sufficient NOE restraints for side chains of these residues. The analysis of side-chain RDCs described above indicates that such restraints would be useful in defining the side-chain conformations of these relatively rigid groups in the solution structure. The RDCs for the Asn and Gln NH_2 groups were calculated for each of the family of 50 NMR solution structures of 1E8L, and these were compared with the experimental values. Figure 3 shows that the Asn 27 and Asn 39 side chains in the family of solution structures are limited to two main orientations related by a 180° rotation of χ^2. In both cases one of these orientations about χ^2 predicts a sum of ^1H–^{15}N RDCs in line with the experimentally observed value and this allows this subset of the side-chain structures to be selected from the larger family of 50 structures. In future structure refinements, χ^2 and χ^3 torsion angle restraints based on the RDCs can be used to improve the definition of Asn and Gln side-chain conformations, respectively.

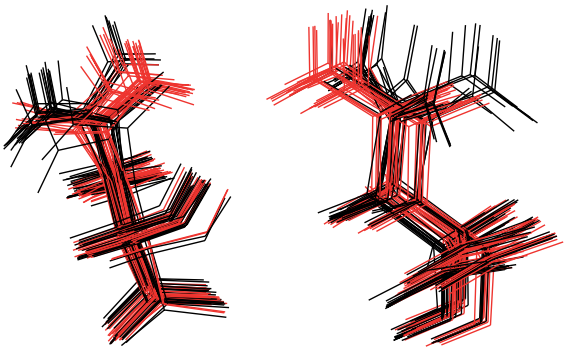

Figure 3. Superposition of the Asn 27 and Asn 39 side chains in a family of 50 NMR structures of hen lysozyme (Schwalbe et al., 2001). Those structures for which the predicted sum of ^{15}N–^{1}H RDCs is within ± 6 Hz and ± 2 Hz for Asn 27 and Asn 39, respectively, are shown in red.

Comparison of RDCs for Asn/Gln side chains with $S^2 < \sim 0.5$

The second group of residues to be analysed are those whose side chains are known from the ^{15}N relaxation study to be very mobile, that is residues with a heteronuclear NOE ratio that is close to zero or negative and $S^2 < \sim 0.5$. In hen lysozyme these are Gln 41, Asn 77, Asn 103, Asn 113 and Gln 121. The RDCs predicted for these side chains in the 14 selected X-ray structures are shown in Table 2. The first three of these residues all have relatively small measured values for the sum of the $^{1}H^{N}$–^{15}N dipolar couplings (|RDC| < 6 Hz) and small, unresolved, ^{1}H–^{1}H dipolar couplings. The values predicted for these residues from the 14 X-ray crystal structures show a great deal of variation; both large and small positive and negative values are predicted for each of these residues. Overlaid crystal structures for these three residues are shown in Figure 2(b). The side chains show a range of orientations in the family of crystal structures and these may reflect the range of conformations adopted in solution. The small observed experimental RDC values reflect the result of the averaging of the RDCs of the multiple conformations sampled in solution. Both Asn 77 and Asn 103 show averaging about χ^1 in solution as reflected by the H^{α}–H^{β} coupling constants (Smith et al., 1991; Bartik and Redfield, 1993). Gln 41 shows a fixed χ^1 value in solution (Smith et al., 1991; Bartik and Redfield, 1993). This is consistent with the X-ray structures which show a single χ^1 conformation and variation about χ^2 and χ^3.

The average B-factors observed in X-ray structures for Asn 77 and Asn 103 are 32.5 ± 14.4 Å^2 and 35.0 ± 13.6 Å^2, respectively. These values are higher than the values observed for the Asn and Gln residues with fixed side-chain orientations described in the previous section and are consistent with substantial side-chain mobility. A lower average B-factor of 22.3 ± 8.4 Å^2 is observed for Gln 41. This value is similar to those observed for the side chains of Asn 59 (18.9 ± 6.9 Å^2) and Asn 74 (17.9 ± 4.9 Å^2) which have a fixed side-chain orientation. Although the side chain of Gln 41 adopts different orientations in the four crystal forms (Figure 2b) each of these orientations is defined by specific intermolecular contacts. The tetragonal crystal is characterised by a large number of intermolecular contacts between Gln 41 and Asn 65, Asp 66, Cys 80 and Ser 81 (Moult et al., 1976). The triclinic, orthorhombic and monoclinic structures show intermolecular contacts to Gln 121, to Arg 21, and to Asn 19 and Ser 24, respectively (Moult et al., 1976; Rao and Sundaralingam, 1996; Oki et al., 1999). In aqueous solution these intermolecular contacts do not exist for Gln 41 and the side chain is very mobile as demonstrated by the low S^2 value and the averaging of the RDCs.

Asn 113 and Gln 121 have larger measured values for the sum of the $^{1}H^{N}$–^{15}N dipolar couplings and large ^{1}H–^{1}H dipolar couplings. The experimental values are not consistent with the values predicted from the 14 X-ray crystal structures. For Asn 113, the overlaid structures show that this side chain is well defined in the crystal structures (Figure 2b). The average $N^{\delta 2}$ and $O^{\delta 1}$ B-factor of 21.5 ± 9.3 Å^2 is consistent with a relatively fixed position for the side chain of Asn 113 in the crystals. The 1LSC and 5LYMa side chains are rotated by 180° about χ^2 with respect to the other structures. In contrast to the fixed χ^1 value seen in the X-ray structures, some averaging about χ^1 is observed in solution (Bartik and Redfield, 1993). The very low heteronuclear NOE value, 0.02 at 60 MHz, observed for Asn 113 is not consistent with a well-defined side-chain conformation. The apparent discrepancy is likely to arise from the contacts made by the side

chain of Asn 113 in the crystal structures. In several tetragonal and triclinic structures $N^{\delta 2}$ is found to be involved in contacts with chloride, bromide or iodide counter-ions from the crystallisation buffer (Vaney et al., 1996; Lim et al., 1998; Steinrauf, 1998; Walsh et al., 1998; Dauter et al., 1999; Sauter et al., 2001). This specific interaction, which is responsible for the fixed side-chain conformation, is unlikely to exist in solution. The larger RDC values observed for Asn 113 indicate that these couplings are not significantly averaged by the mobility of the Asn 113 side chain in contrast to Gln 41, Asn 77 and Asn 103. A large RDC can be produced for a mobile side chain by some conformational restriction; 50% of conformational space maps to a positive RDC and 50% to a negative one. Thus, steric restrictions on the conformational space sampled by a side chain can be such that they favour the positive over the negative RDC space, or vice versa. Furthermore, the ^{15}N–^{1}H and ^{1}H–^{1}H vectors sample different orientations, thus making it possible to see different degrees of averaging for these RDCs.

For Gln 121, the overlaid crystal structures show that this side chain adopts a very wide range of conformations in the crystal structures. Electron density for this side chain is very poorly defined in a number of structures (Moult et al., 1976; Vaney et al., 1996; Carter et al., 1999; Sauter et al., 2001). In the 0.92 Å 3LZT and 4LZT triclinic structures the electron density suggests multiple conformations and the two alternative conformations reported were chosen from many possible ones (Walsh et al., 1998). The average $N^{\varepsilon 2}/O^{\varepsilon 1}$ B-factor for this side chain is 44.7 ± 16.3 $Å^2$ in the family of X-ray structures. The structures predict a range of positive and negative values for the dipolar couplings which are generally not consistent with the experimental data. The 1HEL, 1LSC, 4LZT and 5LYMb structures give predicted values for both the ^{15}N–^{1}H and ^{1}H–^{1}H RDCs that roughly correspond to the experimental values. However, these structures are found to have widely varying χ^2 and χ^3 values as indicated in Figure 2b. These crystal structures may represent the region of conformational space sampled by this side chain in solution. Molecular dynamics simulations show mobility about all χ torsion angles, but also the formation of transient hydrogen bonds to Ser 24, Asp 119 and Arg 125 which are seen in some of the crystal structures (Smith et al., 1995). These may give rise to torsion angle preferences which result in incomplete sampling of conformational space and consequent incomplete averaging of the RDCs, as is observed for Asn 113.

Comparison of RDCs for Asn/Gln side chains with intermediate S^2 values

The third group of residues to be analysed are those whose side chains show intermediate mobility in the ^{15}N relaxation study, that is residues with a heteronuclear NOE ratio between 0.3 and 0.75 and S^2 values between 0.4 and 0.7. In hen lysozyme these are Asn 19, Asn 37, Asn 44, Asn 46, Asn 65, Asn 93 and Asn 106. The RDCs predicted for these side chains in the 14 selected X-ray crystal structures are shown in Table 3 and the X-ray structures are superimposed in Figure 2c. For Asn 19 and Asn 44 a range of side-chain orientations is observed in the crystal structures. Asn 37, Asn 46, Asn 65, Asn 93 and Asn 106 all adopt similar side-chain conformations in the crystal structures and the main difference between the structures is a rotation of 180° about χ^2, resulting from ambiguity in the identification of $N^{\delta 2}$ and $O^{\delta 1}$.

Asn 19 and Asn 44 both have relatively small ($|< 5.5$ Hz$|$) measured values for the sum of the $^{1}H^{N}$–^{15}N dipolar couplings and small ^{1}H–^{1}H dipolar couplings, a similar pattern to that observed for some of the very mobile residues discussed in the previous section. Overlaid X-ray structures for Asn 19 show a range of orientations in the family of crystal structures and an average B-factor for the $N^{\delta 2}$ and $O^{\delta 1}$ atoms of 29.4 ± 12.2 $Å^2$; this suggests that this side chain is mobile in the crystal. The RDC values predicted for this residue do not show any pattern or correlation with the experimental data. In solution averaging about χ^1 is observed for Asn 19 (Smith et al., 1991). Therefore, it can be concluded that the side chain of Asn 19 is mobile in solution.

Asn 44 is found to adopt conformations in the X-ray structures that are dependent on the crystal symmetry. Two conformations are observed in all the tetragonal structures analysed; these are related by a 180° rotation about χ^2. One of these orientations gives rise to a hydrogen

bond between Asn 44 $H^{\delta 21}$ and Gln 57 $O^{\varepsilon 1}$. However, neither orientation observed in the tetragonal structures gives predicted RDC values that agree with the experimental data. The orthorhombic and triclinic structures adopt a very different conformation with a hydrogen bond between Asn 44 $H^{\delta 21}$ and Asp 52 $O^{\delta 2}$. The monoclinic structures adopt two further conformations both lacking hydrogen bonds. None of the orientations found in the triclinic, orthorhombic or monoclinic crystals is found to give good agreement with the measured dipolar couplings. The fixed orientation of Asn 44 in the tetragonal crystals reflects the intermolecular crystal contacts between Asn 44 $N^{\delta 2}$ and Arg 45 $N^{\varepsilon 1}$ and Arg 68 $N^{\varepsilon 1}$ which are not observed in the triclinic, monoclinic or orthorhombic structures (Moult et al., 1976). The average B-factor observed for Asn 44 is 26.4 ± 6.5 Å^2. This value is lower than the B-factors observed for the mobile residues Asn 19, 77, 103 and Gln 121 and may reflect the decrease in mobility arising from the intermolecular contacts observed for Asn 44. In solution, Asn 44 shows averaging about χ^1 (Bartik and Redfield, 1993) and the RDC data indicate that, as in the case of Asn 19, significant mobility of the $CONH_2$ moiety occurs.

For Asn 37 the majority of crystal structures give good agreement between the experimental and predicted dipolar couplings. Asn 37 forms a hydrogen bond between $O^{\delta 1}$ and Lys 33 N^{ζ} in all these X-ray structures. The Asn 37 χ^2 orientation is incorrect in the 1LSC and 5LYMb structures and these structures are missing the hydrogen bond to Lys 33 and instead show steric clashes between the Asn 37 NH_2 and Lys 33 NH_3^+ groups. A 180° rotation about χ^2 leads to predicted dipolar couplings that are consistent with the experimental data, the formation of the hydrogen bond and the absence of steric clashes. The H^{α}–H^{β} coupling constants for Asn 37 indicate some averaging about χ^1 in solution but this averaging is not as extensive as that observed for more mobile residues such as Asn 19 and Asn 77 (Smith et al., 1991). The molecular dynamics simulation of hen lysozyme (Smith et al., 1995) shows mobility about both χ^1 and χ^2 for Asn 37, but also quite persistent hydrogen bonding to Lys 33 N^{ζ} (17% population within an 800 ps trajectory). Individual structures taken from the molecular dynamics simulation show Asn 37 in two different conformations. One of these is identical with that found in the crystal structures, forming the hydrogen bond to Lys 33. The other conformation also forms a hydrogen bond to Lys 33, but with different χ^1 and χ^2 torsion angles. The predicted ^{15}N–^1H and ^1H–^1H RDCs of the former conformation fit the experimental ones well (22.4 Hz and 31.6 Hz, respectively), the others do not (6.2 Hz and 3.7 Hz, respectively). Thus, it appears that the side-chain orientation observed for Asn 37 in the majority of crystal structures is also the dominant conformation in solution. The observation that the RDCs are somewhat smaller than the predicted values indicates that there is mobility about this average conformation; this is consistent with the observed S^2 value of 0.51 (Buck et al., 1995). The average B-factor observed for Asn 37 is 25.4 ± 5.6 Å^2. This is higher than the values of 12.4 ± 3.0 to 18.9 ± 6.9 Å^2 observed for the residues with S^2 values above 0.7 and is consistent with greater mobility for this side chain.

For Asn 93 approximately half of the crystal structures have a side-chain orientation that gives good agreement with the experimental RDCs. Asn 93 does not form any stable hydrogen bonds other than to water; this would make the N^{δ} and O^{δ} assignment in X-ray diffraction data difficult. However, the structures that give poor agreement with the experimental data, 1RFP, 1HEL, 1DPX, 1AZF, 1AKI and 5LYMa/b all show a severe steric clash between their $H^{\delta 2}$ and H^{α} atoms when hydrogens are added to the structure. A 180° rotation about χ^2 for these structures removes this steric clash and gives predicted RDCs that are consistent with the experimental data. The program Reduce (Word et al., 1999a) is able to identify this clash in each structure and suggests a 180° rotation about χ^2. The side-chain orientation observed in the two neutron diffraction structures, in which the N^{δ} and O^{δ} positions are readily distinguished, gives good agreement with the experimental RDC values. Asn 93 shows a fixed orientation about χ^1 in solution (Smith et al., 1991; Bartik and Redfield, 1993). Thus, the average conformation of the Asn 93 side chain in solution is consistent with that observed in the neutron structures and in the 193L, 1LSC, 1LZA, 1IEEb, 1LKS, 4LZT and 1BGI X-ray structures.

Asn 46 is in close proximity to Asn 59, and when both these side chains are in the orientation which agrees with the RDC data, they should have their NH_2 groups pointing towards each other. The Asn 46 side chain is found to be oriented in this way only in the 1RFP, 1IEEb, 1LKS, 4LZT, 1BGI, 5LYMa and 5LYMb structures. The other structures all show their Asn 46 side chain in the incorrect orientation. However, although a simple rotation of the Asn 46 χ^2 angle by 180° is possible for the 1AKI structure, this is not possible for the 193L, 1HEL, 1LSC, 1LZA, 1DPX and 1AZF structures due to steric hindrance between the Asn 46 and 59 NH_2 groups. Asn 46 is located in the turn between β-strands 1 and 2 which shows a large RMSD in the family of crystal structures; this is reflected in the relatively poor overlay of this residue shown in Figure 2c. Consequently the environment of the Asn 46 side chain varies in the different X-ray structures, depending in part on the position of the backbone in the turn. Most of the structures in which the Asn 46 side-chain orientation does not agree with the RDC data and cannot be rotated by 180° were obtained from tetragonal crystals. This suggests that the packing of molecules in the tetragonal crystals may change the position of the β-turn enough to force the Asn 46 side chain to adopt the alternate orientation of its $CONH_2$ group due to steric constraints. An examination of the hydrogen bonds present is difficult, with large variations between the different crystal structures. In some cases Asn 46 can hydrogen bond with its two H^{δ} atoms to Asp 52 $O^{\delta 1/2}$ and Ser 50 O^{γ}. While the crystal structures do not present a coherent view of the orientation of Asn 46 and its surroundings, the RDC data are clear about the solution conformation, and show the two Asn 46 and 59 NH_2 groups to be facing each other.

For Asn 65 the majority of the structures have a side-chain orientation that is consistent with the experimental data. The 1AZF and 5LYMa Asn 65 side chains are in the alternate conformation and give predicted dipolar couplings that fit less well with the experimental data. However, as the sum of the $^1H^N$–^{15}N dipolar couplings is of the correct sign it is more difficult to rule out this orientation. Asn 65 O^{δ} forms a weak hydrogen bond to Gly 67 H^N in most of the X-ray structures that are consistent with the RDC data. Asn 65 shows a fixed orientation about χ^1 in solution. Although the molecular dynamics simulation shows some fluctuations about χ^2 for this residue, an investigation of individual structures taken from different time points throughout the simulation indicates that these are merely fluctuations about the average position which would form the hydrogen bond to Gly 67. The program Reduce (Word et al., 1999a) also favours the side-chain orientation that fits the RDC data best and this orientation is also observed in the 1LZN neutron structure. Thus, in solution the Asn 65 side adopts an average conformation that is the same as in the majority of crystal structures.

For Asn 106, the majority of structures give a predicted sum of the ^{15}N–^1H dipolar couplings that is of the same sign and similar magnitude as the experimental value. However, these structures predict a large ^1H–^1H RDC (~ 20 Hz) that is not observed experimentally; calculations indicate that contributions from other nearby protons are not responsible for the observed decrease in the ^1H–^1H RDC. The orientation of the Asn 106 side chain in the 1LSC, 4LZT and 1BGI structures show a 180° rotation about χ^2 relative to the other structures and in the 1LKS structure shows a slightly smaller rotation about χ^2. The former three structures show better agreement with the ^1H–^1H RDC but worse agreement with the ^{15}N–^1H RDC. Thus, none of the 14 X-ray structures analysed can predict the RDC data adequately. Asn 106 is involved in intermolecular contacts in both the tetragonal and triclinic structures and these may be responsible for the observed side-chain orientation (Moult et al., 1976; Steinrauf, 1998; Walsh et al., 1998). The average B-factor of 18.9 ± 9.9 $Å^2$ observed for Asn 106 is consistent with reduced mobility in the crystal arising from these contacts. In the high resolution (0.95 Å) 4LZT triclinic structure, however, the density of the Asn 106 side chain is unclear indicating mobility (Walsh et al., 1998). In the low temperature (120 K) 3LZT triclinic structure two alternative conformations are identified for Asn 106 suggesting that the unclear density observed at 295 K arises from multiple conformations (Walsh et al., 1998). Peak shape analysis shows χ^1 to be fixed in solution (Bartik and Redfield, 1993). Thus, it appears that in

solution the side chain of Asn 106 is not fixed beyond the C^{β} position and that the observed RDCs reflect the mobility of the side-chain amide group.

Scaling the predicted RDCs using experimental order parameters (S^2)

Nine residues, Asn 27, 37, 39, 46, 59, 65, 74, 93 and Gln 57, show experimental RDCs that are consistent with a single, relatively fixed, side-chain orientation in solution. For eight of these nine residues the experimental ^{15}N–^{1}H and ^{1}H–^{1}H RDCs are found to be smaller in magnitude than the average values predicted from the 14 X-ray crystal structures analysed here (Tables 1 and 3). This is illustrated in Figure 4 which shows a plot of the experimental versus predicted sum of ^{15}N–^{1}H RDCs; a correlation coefficient, R, of 0.97 and a slope of 0.79 are obtained for the nine residues. The deviation of the slope from the expected value of 1.0 arises because the experimental RDCs are generally smaller than the predicted values. This reduction in the experimental RDCs may be the result of fast motions of the side-chain groups. The residual dipolar coupling between two nuclei X and Y is given by

$$D_{xy} = S\mu_0\gamma_x\gamma_y h[A_a(3\cos^2\theta - 1) + 3/2A_r(\sin^2\theta\cos 2\phi)]4\pi^2 r_{xy}{}^3,$$

where S is the generalised order parameter for internal motion of the XY vector, μ_0 is the magnetic permeability of vacuum, γ_x and γ_y are the magnetogyric ratios of X and Y, h is Planck's constant, r_{xy} is the distance between X and Y, A_a and A_r are the axial and rhombic components of the alignment tensor, and θ and ϕ are cylindrical coordinates describing the orientation of the vector XY in the principal axis system of the alignment tensor (Tjandra and Bax, 1997). For backbone RDCs the order parameter, S, is usually approximated to be uniform for all residues and to be equal to 1. Order parameters, S^2, have been measured previously for the Asn and Gln side chains of hen lysozyme (Buck et al., 1995). These are reported to vary from 0.51 to 0.82 for this group of 9 residues. The square root of these order parameters can be used in the calculation of RDCs from the crystal structures using the equation defined above. The experimental sum of ^{15}N–^{1}H RDCs are plotted as a function of the 'S-corrected' predicted RDC values in Figure 4; in this case a correlation coefficient of 0.98 and a slope of 0.98 are obtained. Thus, the inclusion of the experimental order parameter in the calculation of RDCs from X-ray coordinates leads to improved agreement with experimental RDCs. If experimental S^2 values are available then it will be important to use these to correct experimental RDC values for side chains before these are included as restraints in structure refinement.

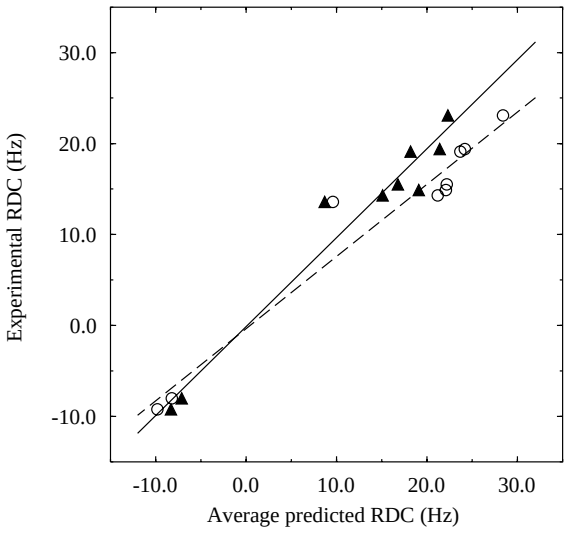

Figure 4. Comparison of experimental and predicted RDCs. The sum of the experimental ^{15}N–^{1}H RDCs for the nine residues found to have a fixed side-chain orientation are plotted on the vertical axis. The average of the ^{15}N–^{1}H RDC sum predicted from 14 X-ray crystal structures is plotted on the horizontal axis; open circles represent RDCs that have been calculated with $S = 1$ and filled triangles represent RDCs calculated using the experimental S values (Buck et al., 1995). A correlation coefficient of 0.97 and a slope of 0.79 are found for the RDCs calculated with $S = 1$. A correlation coefficient of 0.98 and a slope of 0.98 are found for the RDCs calculated using the experimental S values. The order parameters reported previously were calculated using an N–H bond length of 1.02 Å (Buck et al., 1995). These order parameters increase by $\sim$ 10–12% if the N–H bond length is increased from 1.02 to 1.04 Å. This increase in the values of S^2 leads to a slope of 0.93 in the plot of experimental *versus* 'S-corrected' RDCs.

Conclusions

Experimental ^{15}N–^{1}H and ^{1}H–^{1}H RDCs for the Asn and Gln side chains of hen lysozyme have been analysed in conjunction with ^{15}N relaxation data for the side-chain NH_2 groups, information

about χ^1 torsion angles in solution obtained from H^{α}–H^{β} coupling constants and COSY peak-shape analysis, molecular dynamics simulations and a family of 16 high resolution X-ray and neutron diffraction structures. This has provided insights into the effects of dynamics on the measured RDCs and the suitability of using side-chain RDCs as restraints in structure refinement. It has also allowed us to address issues concerning the accuracy of X-ray structures for Asn and Gln side-chain amide groups.

The very large number of high resolution crystal structures available for lysozyme has made it possible to distinguish between two distinct groups of asparagine and glutamine side chains. The first group contains residues whose side chains show a fixed, relatively rigid, conformation in solution. For these residues there is reasonably good agreement between the experimental RDCs and those predicted from the crystal structures. There are nine residues in this category: Asn 27, 39, 59, 74 and Gln 59 have side-chain S^2 values of greater than 0.7 and a similar mobility to backbone amides in solution; Asn 37, 46, 65 and 93 have intermediate values of S^2 ranging from 0.51 to 0.62. These latter residues are, therefore, more mobile than backbone amides in solution. However, despite this increased mobility these residues still show a preferred side-chain orientation.

The second group contains residues whose side chains do not adopt a single, well-defined, conformation in solution. These residues do not show a correlation between the experimental and predicted RDCs. In many cases the family of crystal structures shows a range of orientations for these side chains and, as a result, different calculated RDCs. There are eight residues in this category: Gln 41 and 121, and Asn 77, 103 and 113 have S^2 values of less than 0.5 and heteronuclear NOE ratios that are close to zero or negative, indicative of substantial side-chain mobility; Asn 19, 44 and 106 have intermediate S^2 values, ranging from 0.43 to 0.58, and heteronuclear NOE ratios ranging from 0.3 to 0.6.

For some residues in hen lysozyme, it is possible to predict which of these two groups the side chain belongs to from relaxation data alone. For example, all Asn and Gln residues with side-chain S^2 values of greater than 0.7 are found to have fixed side-chain orientations, and all residues with side-chain S^2 values of less than 0.5 and a heteronuclear NOE ratio of less than 0.1 do not adopt a single orientation in solution. However, for residues with intermediate S^2 and NOE values it is more difficult to determine on the basis of the relaxation data alone if they have a fixed or mobile side chain.

In addition, the X-ray structure cannot always act as a guide. Although in many cases B-factors or overlays of a family of crystal structures can be a good guide to mobility in solution, there are some notable exceptions. For example, several residues that do not adopt a single well-defined side-chain orientation in solution, such as Asn 44, Asn 106 and Asn 113, are found to adopt a well-defined side-chain orientation in a subset or in all of the crystal structures. These side chains are involved in specific interactions in the crystal lattice involving contacts with other lysozyme molecules in the unit cell or with ions present in the crystallisation buffer. The observation from RDCs, ^{15}N relaxation data and coupling constants that these residues are mobile in solution indicates that these crystallographic contacts, and the side-chain orientations that result from them, are not relevant to the solution structure.

The RDC values for mobile residues are expected to be small or close to zero due to conformational averaging of the side-chain. This behaviour is indeed observed experimentally for many residues in the mobile category. However, for some residues, including Asn 106, Asn 113 and Gln 121, larger values are measured for one or both RDC despite substantial conformational flexibility. This may be the result of steric restrictions on the side-chain orientation. This observation that mobility does not always lead to complete averaging of RDCs to zero is important to note because it means that the observation of a large RDC may not necessarily reflect a fixed side-chain conformation as supposed by Bertini et al. (2000). It is essential to use measured order parameters or heteronuclear NOE ratios to assess the side-chain mobility before using an experimental RDC as a structural restraint.

A further point regarding RDCs and dynamics relates to the group of Asn and Gln residues with relatively rigid side chains. It has been suggested that RDCs may need to be scaled by more than just the order parameter determined by ^{15}N relaxation methods, as the window of timescales

probed by RDCs is larger than that of standard ^{15}N relaxation studies (Meiler et al., 2001; Tolman et al., 2001; Peti et al., 2002; Tolman, 2002). However, good agreement is found in this study between the experimental RDC values and those predicted from X-ray structures when the experimental S^2 value is included in the calculation. This suggests that these residues are unlikely to experience significant additional dynamics on slower timescales that would lead to further scaling of the RDCs (Meiler et al., 2001; Tolman et al., 2001; Peti et al., 2002; Tolman, 2002).

It is important to consider side-chain RDCs in the light of relaxation data which give an indication of mobility, as it is only for residues in the 'fixed' category that the RDC will be able to give information about structure. Several reports in the literature suggest using half-open square well penalty functions for side-chain RDCs, in effect setting the measured RDC value as a lower limit in the calculation (Ottiger et al., 1998; Chou et al., 2001; de Alba and Tjandra, 2002).

RDCs for residues whose S^2 value is greater than 0.75 and which can therefore be unambiguously assigned to the 'fixed' category can certainly be used in structure calculations. However, the analysis in which the RDCs are scaled by the S^2 value indicates that, as an alternative to using a half-open square well, it may well be suitable simply to carry out such scaling before using the RDC as a structural restraint in the normal manner.

For residues with intermediate S^2 and NOE values, where it is more difficult to determine on the basis of the relaxation data alone if they have a fixed or mobile side chain, the RDC data must be interpreted with caution. For these residues it may be more appropriate to use the measured RDCs as a filter for the side-chain orientations observed in a family of solution structures rather than as direct structural restraints in the structure calculation, even with a half-open potential restraint.

Comparison of the experimental RDCs with values calculated from the X-ray structures has shown that the similarity between the oxygen and nitrogen electron densities is a limitation to the correct identification of the orientation of Asn and Gln side chains in X-ray crystal structures of 1 Å or worse resolution. Of all 66 structures available for hen lysozyme the four highest resolution structures 4LZT (0.93 Å resolution, 295 K temperature of collection), 1IEE (0.94 Å resolution, 110 K), 3LZT (0.95 Å resolution, 120 K) and 1LKS (1.1 Å resolution) and the 2LZT structure (2.0 Å resolution, 295 K), were the only X-ray structures in which the side-chain conformations of all the nine 'fixed' Asn and Gln residues were in agreement with the experimental RDC data. In all the other X-ray structures a 180° rotation about χ^2 or χ^3, leading to the swapping of $N^{\delta/\varepsilon 2}$ and $O^{\delta/\varepsilon 1}$, was found for at least one Asn or Gln residue. A table summarising the observed Asn/Gln side-chain conformations for all 66 crystal structures is available as Supporting Information.

Asn and Gln side chains are often found at the surface of proteins or in active sites of enzymes and can be involved in important protein-protein or protein-substrate interactions. Therefore, it is important that the orientation of the amide side-chain group is correctly defined in crystal structures. We show here for hen lysozyme that RDC data can be used to identify errors in the assignment of the $N^{\delta/\varepsilon 2}$ and $O^{\delta/\varepsilon 1}$ atoms of Asn and Gln side chains in crystal structures. Word et al. (1999a) have shown that the addition of hydrogen atoms to X-ray structures and the consideration of the van der Waal's interactions resulting from these hydrogen atoms can in many instances help to distinguish between the $N^{\delta/\varepsilon 2}$ and $O^{\delta/\varepsilon 1}$ atoms of Asn and Gln. Their program Reduce (used in conjunction with the programs Probe and Mage) was used to analyse the lysozyme crystal structures. In all cases where the RDC data indicated a swapping of the $N^{\delta/\varepsilon 2}$ and $O^{\delta/\varepsilon 1}$ atoms in a crystal structure, the program Reduce also identified the Asn or Gln side chain as being incorrectly oriented. Therefore, the routine use of Reduce by crystallographers when solving X-ray structures would substantially decrease the number of incorrect Asn and Gln $N^{\delta/\varepsilon 2}$ and $O^{\delta/\varepsilon 1}$ assignments found in high resolution X-ray structures of proteins.

Acknowledgements

This is a contribution from the Oxford Centre for Molecular Sciences which is supported by the U.K. Biotechnology and Biological Sciences Research Council (BBSRC), the Medical

Research Council, and the Engineering and Physical Sciences Research Council. C.R. acknowledges an Advanced Research Fellowship from the BBSRC. V.A.H. was funded by a BBSRC graduate studentship and a bursary from St. Peter's College.

Supporting Information Available: One table (7 pages) summarising the observed Asn/Gln side-chain conformations for all 66 crystal structures of hen egg-white lysozyme. This material is available at: http://kluweronline.com/issn/0925-2738

References

Artymiuk, P.J., Blake, C.C.F., Rice, D.W. and Wilson, K.S. (1982) *Acta Crystallog. Sect. B*, **38**, 778–783.

Bartik, K. and Redfield, C. (1993) *J. Biomol. NMR*, **3**, 415–428.

Bax, A. and Tjandra, N. (1997) *J. Biomol. NMR*, **10**, 289–292.

Berman, H.M., Westbrook, J., Feng, Z., Gilliland, G., Bhat, T.N., Weissig, H., Shindyalov, I.N. and Bourne, P.E. (2000) *Nucl. Acids Res.*, **28**, 235–242.

Bertini, I., Felli, I.C. and Luchinat, C. (2000) *J. Biomol. NMR*, **18**, 347–355.

Blake, C.C.F., Koenig, D.F., Mair, G.A., North, A.C.T., Philips, D.C. and Sarma, V.R. (1965) *Nature*, **206**, 757–761.

Bon, C., Lehmann, M.S. and Wilkinson, C. (1999) *Acta Crystallog. Sect. D*, **55**, 978–987.

Boyd, J. and Redfield, C. (1998) *J. Am. Chem. Soc.*, **120**, 9692–9693.

Brünger, A.T. (1992) *XPLOR Version 3.1: A System for X-Ray Crystallography and NMR*, Yale University Press, New Haven, CT.

Buck, M., Boyd, J., Redfield, C., MacKenzie, D.A., Jeenes, D.J., Archer, D.B. and Dobson, C.M. (1995) *Biochemistry*, **34**, 4041–4055.

Cai, M., Huang, Y. and Clore, G.M. (2001) *J. Am. Chem. Soc.*, **123**, 8642–8643.

Carter, D.C., Lim, K., Ho, J.X., Wright, B.S., Twigg, P.D., Miller, T.Y., Chapman, J., Keeling, K., Ruble, J., Vekilov, P.G., Thomas, B.R., Rosenberger, F. and Chernov, A.A. (1999) *J. Cryst. Grow.*, **196**, 623–637.

Cheetham, J.C., Artymiuk, P.J. and Phillips, D.C. (1992) *J. Mol. Biol.*, **224**, 613–628.

Chou, J.J., Li, S., Klee, C.B. and Bax, A. (2001) *Nat. Struct. Biol.*, **8**, 990–997.

Cornilescu, G., Marquardt, J.L., Ottiger, M. and Bax, A. (1998) *J. Am. Chem. Soc.*, **120**, 6836–6837.

Dauter, Z., Dauter, M., De La Fortelle, E., Bricogne, G. and Sheldrick, G.M. (1999) *J. Mol. Biol.*, **289**, 83–92.

de Alba, E. and Tjandra, N. (2002) *Prog. Nucl. Magn. Reson. Spectrosc.*, **40**, 175–197.

de Alba, E., De Bries, L., Farquhar, M.G. and Tjandra, N. (1999) *J. Mol. Biol.*, **29**, 927–938.

Ho, J.X., Declerq, J.-P., Myles, D.A.A., Wright, B.S., Ruble, J.R. and Carter, D.C. (2001) *J. Cryst. Grow.*, **232**, 317–325.

Imoto, T., Johnson, L.N., North, A.C.T., Phillips, D.C. and Rupley, J.A. (1972) In *The Enzymes*, P.D. Boyer (Ed.), Academic Press, New York, 665–868.

Koradi, R., Billeter, M. and Wüthrich, K. (1996) *J. Mol. Graph.*, **14**, 51–55.

Kurinov, I.V. and Harrison, R.W. (1995) *Acta Crystallog. Sect. D*, **51**, 98–109.

Lesk, A.M. (2001) *Introduction to Protein Architecture*, Oxford University Press, New York.

Lim, K., Nadarajah, A., Forsythe, E. and Pusey, M.L. (1998) *Acta Crystallog. Sect. D*, **54**, 899–904.

MacKenzie, D.A., Spencer, J.A., Le Gal-Coeffet, M.F. and Archer, D.B. (1996) *J. Biotechnol.*, **46**, 85–93.

Maenaka, K., Matsushima, M., Song, H., Sunada, F., Watanabe, K. and Kumagai, I. (1995) *J. Mol. Biol.*, **247**, 281–293.

Markus, M.A., Gerstner, R.B., Draper, D.E. and Torchia, D.A. (1999) *J. Mol. Biol.*, **292**, 375–387.

Mason, S.A., Bentley, G.A. and McIntyre, G.J. (1984) *Basic Life Sci.*, 27, 323–334.

McRee, D.E. (1999) *Practical Protein Crystallography*, Academic Press, San Diego, U.S.A.

Meiler, J., Prompers, J.J., Peti, W., Griesinger, C. and Brüschweiler, R. (2001) *J. Am. Chem. Soc.*, **123**, 6098–6107.

Meissner, A., Duus, J.Ø. and Sørensen, O.W. (1997) *J. Magn. Reson.*, **128**, 92–97.

Motoshima, H., Mine, S., Masumoto, K., Abe, Y., Iwashita, H., Hashimoto, Y., Chijiiwa, Y., Ueda, T. and Imoto, T. (1997) *J. Biochem. (Tokyo)*, **121**, 1076–1081.

Moult, J., Yonath, A., Traub, W., Smilansky, A., Podjarny, A., Rabinovich, D. and Sya, A. (1976) *J. Mol. Biol.*, **100**, 179–195.

Niimura, N., Minezaki, Y., Nonaka, T., Castagna, J.-C., Cipriani, F., Hogoj, P., Lehmann, M.S. and Wilkinson, C. (1997) *Nat. Struct. Biol.*, **4**, 909–914.

Oki, H., Matsuura, Y., Komatsu, H. and Chernov, A.A. (1999) *Acta Crystallog. Sect. D*, **55**, 114–121.

Ottiger, M. and Bax, A. (1999) *J. Biomol. NMR*, **13**, 187–191.

Ottiger, M., Delaglio, F. and Bax, A. (1998) *J. Magn. Reson.*, **131**, 373–378.

Permi, P. (2001) *J. Magn. Reson.*, **153**, 267–272.

Peti, W., Meiler, J., Brüschweiler, R. and Griesinger, C. (2002) *J. Am. Chem. Soc.*, **124**, 5822–5833.

Prestegard, J.H. (1998) *Nat. Struct. Biol.*, **5**(Suppl.), 517–522.

Rao, S.T. and Sundaralingam, M. (1996) *Acta Crystallog. Sect. D*, **52**, 170–175.

Richardson, D.C. and Richardson, J.X. (1992) *Protein Sci.*, **1**, 3–9.

Richardson, D.C. and Richardson, J.S. (1994) *Trends Biochem. Sci.*, **19**, 135–138.

Sauter, C., Otálora, F., Gavira, J.-A., Vidal, O., Giergé, R. and García-Ruiz, J.M. (2001) *Acta Crystallog. Sect. D*, **57**, 1119–1126.

Schwalbe, H., Grimshaw, S.B., Spencer, A., Buck, M., Boyd, J., Dobson, C.M., Redfield, C. and Smith, L.J. (2001) *Protein Sci.*, **10**, 677–688.

Smith, L.J., Mark, A.E., Dobson, C.M. and van Gunsteren, W.F. (1995) *Biochemistry*, **34**, 10918–10931.

Smith, L.J., Sutcliffe, M.J., Redfield, C. and Dobson, C.M. (1991) *Biochemistry*, **30**, 986–996.

Steinrauf, L.K. (1998) *Acta Crystallog. Sect. D*, **54**, 767–779.

Tjandra, N. and Bax, A. (1997) *Science*, **278**, 1111–1114.

Tjandra, N., Omichinski, J.G., Gronenborn, A.M., Clore, G.M. and Bax, A. (1997) *Nat. Struct. Biol.*, **4**, 732–738.

Tolman, J.R. (2002) *J. Am. Chem. Soc.*, **124**, 12020–12030.

Tolman, J.R., Al-Hashimi, H.M., Kay, L.E. and Prestegard, J.H. (2001) *J. Am. Chem. Soc.*, **123**, 1416–1424.
Vaney, M.C., Maignan, S., Riès-Kautt, M. and Ducruix, A. (1996) *Acta Crystallog. Sect. D*, **52**, 505–517.
Vocadlo, D.J., Davies, G.J., Laine, R. and Withers, S.G. (2001) *Nat.* **412**, 835–838.
Walsh, M.A., Schneider, T.R., Sieker, L.C., Dauter, Z., Lamzin, V.S. and Wilson, K.S. (1998) *Acta Crystallog. Sect. D*, **54**, 522–546.
Weiss, M.S., Palm, G.J. and Hilgenfeld, R. (2000) *Acta Crystallog. Sect. D*, **56**, 952–958.
Wilson, K.P., Malcolm, B.A. and Matthews, B.W. (1992) *J. Biol. Chem.*, **267**, 10842–10849.
Word, J.M., Lovell, S.C., Richardson, J.S. and Richardson, D.C. (1999a) *J. Mol. Biol.*, **285**, 1735–1747.
Word, J.M., Vovell, S.C., LaBean, T.H., Taylor, H.C., Zalis, M.E., Presley, B.K., Richardson, J.S. and Richardson, D.C. (1999b) *J. Mol. Biol.*, **285**, 1711–1733.